Effects of Long Rarefied Plasma inside Cone on Fast Electron Generation for FIREX-I Targets

H. Sakagami[1], A. Sunahara[2], T. Johzaki[2], and H. Nagatomo[3]

[1]Fundamental Physics Simulation Div., National Inst. for Fusion Science, Toki, Japan
[2]Institute for Laser Technology, Suita, Japan
[3]Institute of Laser Engineering, Osaka University, Suita, Japan

sakagami.hitoshi@nifs.ac.jp

Abstract. Long-scale pre-plasmas are generated inside the cone by the pre-pulse of the heating laser in cone-guided fast ignition scheme and it is found that the energy coupling rate from the laser to fast electrons especially suitable for core heating is drastically reduced by preformed plasmas. To mitigate this serious problem, an extremely thin film is suggested to cover an entrance of the cone. This method introduces long rarefied plasmas inside the cone, which could affect fast electron characteristics produced by the main pulse. Therefore, effects of long rarefied plasmas on fast electron generation are investigated and it is found that the electron beam intensity becomes larger than that without the rarefied plasma, but coupling efficiency from the heating laser to the core decreases due to lack of appropriate electrons for core heating. If the length the rarefied plasma is 500 μm and 10 % degradation of the core electron temperature is acceptable, the thin film must be expanded by irradiation of the pre-pulse so that the density of the remnant rarefied plasma becomes than $0.1n_{cr}$.

1. Introduction

The FIREX-I project [1] aims to demonstrate that the imploded core could be heated up to the ignition temperature, 5 keV, and incorporated experiments for FIREX-I, in which heating is combined with implosion, have started at Institute of Laser Engineering, Osaka University. Efficient heating mechanisms and achievement of such high temperature have not been, however, clarified yet, and we have been promoting the Fast Ignition Integrated Interconnecting code (FI^3) project to boldly explore fast ignition frontiers [2-7]. First series of the incorporated experiments have been performed in 2009, and only 30-fold enhancement in neutron yield, which was ~ 1/30 smaller than that in 2002 experiments [8], was achieved and lower energy coupling from the heating laser to the imploded core was expected [9]. According to two-dimensional core heating simulations where uniform core heating rate was assumed, an energy coupling rate of the heating laser to the compressed core could be estimated around 20 % in 2002 experiments, but less than 5 % in 2009 experiments [10]. An unavoidable pre-pulse of the heating laser generates long-scale low-density plasmas (preformed plasmas) inside the cone. A main pulse of the heating laser has to interact with these long-scale preformed plasmas and it results in increasing the distance from the generation point of fast electrons to the core and generating too energetic fast electrons [11]. In turn, low energy fast electrons especially suitable for core heating decease and it leads to low energy coupling.

To mitigate the preformed plasma effects, an entrance of the cone is suggested to be covered with an extremely thin film. The pre-pulse could be interrupted and absorbed by this film, and cannot irradiate the cone wall to produce the preformed plasmas. But inside of the cone is filled up with rarefied plasmas, which are the residue of expanding thin film plasmas. The main pulse of the heating laser must propagate through very long (>500 μm) rarefied ($<<n_{cr}$) plasmas. However there has been few research using such long rarefied plasmas, and we have investigated effects of long rarefied plasmas on core heating with the use of FI^3, which consists of two radiation-hydro codes, PINOCO [12] for implosion and STAR-2D [13] for pre-plasma formation, two Particle-in-Cell codes, FISCOF [14] and ASCENT [15] for relativistic

laser-plasma interaction and one Fokker Planck-hydro code FIBMET [16] for core heating process.

2. Suppression of Preformed Plasma

2.1 Pre-pulse and Preformed Plasma

The plasma profile inside the cone was measured by X-ray pinhole images in 2009 experiments [17]. The time-integrated X-ray image shows a wide bright area at ~100 μm away from the cone tip. It means that the heating laser is absorbed far away from the cone tip even it is focused at the center of the cone, and indicates that the inside of the cone is filled with preformed plasmas, which are generated by the pre-pulse. To estimate the pre-pulse level, we compared STAR-2D simulation results with experimental data [18]. When the laser intensity in the simulation is 10^{13} W/cm^2, the density scale length of the preformed plasma is measured as 100 μm and the blow off speed of electrons as $1x10^7$ cm/s at 1 ns. These values are in good agreement with experimental observations, and we can conclude that the cone is illuminated by the pre-pulse of the heating laser with 10^{13} W/cm^2 intensity and 1 ns duration before it is irradiated by the main pulse. The corresponding pre-pulse energy is estimated to be 130 mJ. For the next step, we also simulated the pre-plasma formation inside the cone with STAR-2D [18]. The temporal profile of the laser is flattop with 1 ns duration, and the wavelength and the spot diameter are set to 1.06 μm and 40 μm (Gaussian FWHM), respectively. The tip diameter of the cone is 30 μm. Preformed plasma profiles are shown in Figure 1 for different intensities ($1x10^{11}$, $1x10^{12}$ and $1x10^{13}$ W/cm^2) and different open angles (30, 45 and 60 degree). For the pre-pulse intensity estimated above and the open angle in 2009 experiments (30 or 45 degree), the preformed plasma expands to the overall inner space of the cone. As the cone with a larger open angle has a larger volume to be filled, the density scale length of the preformed plasma is reduced when the open angle of the cone increases. While the critical density ($n_e=10^{21}$ cm^{-3} for 1.06 μm laser) point is still close to the cone tip, low-density preformed plasmas with long-scale length exist inside the cone and the main pulse of the heating laser must interact with these plasmas.

To evaluate preformed plasma effects inside the cone, we carried out ASCENT-2D simulations [10]. The Au cone (Z=40, $100n_{cr}$, 30 degree open angle, 12 μm tip inner width, 5 μm tip

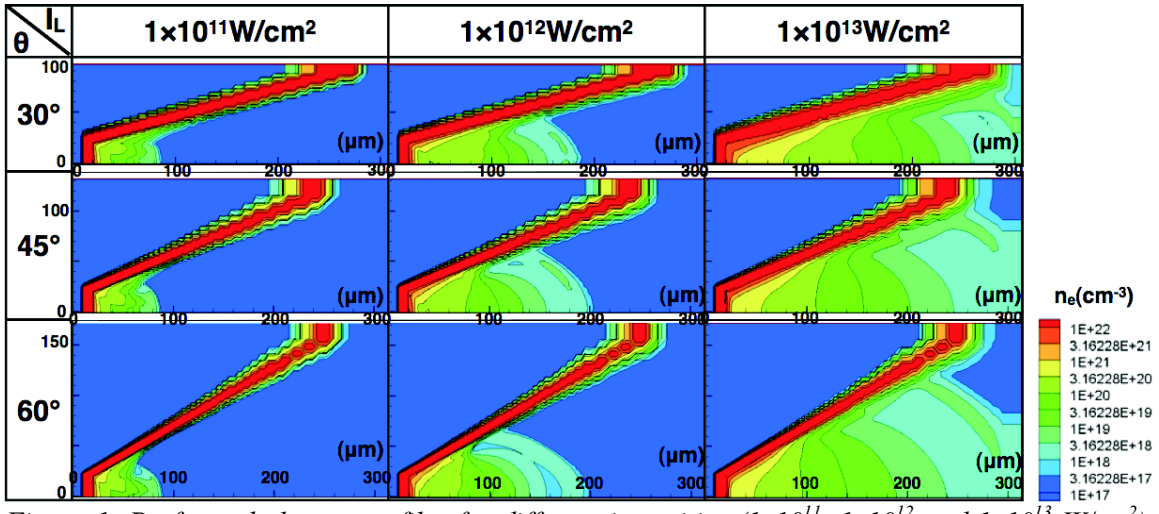

Figure 1: Preformed plasma profiles for different intensities ($1x10^{11}$, $1x10^{12}$ and $1x10^{13}$ W/cm^2) and different open angles (30, 45 or 60 degree).

thickness and 8 μm side wall thickness) is surrounded by imploded CD plasma (Z=3.5 and $50n_{cr}$). As the case without preformed plasmas, surface plasmas with the short scale length (1 μm) from $100n_{cr}$ to $0.1n_{cr}$ are introduced in front of the cone tip. According to preformed plasma characteristics in Figure 1 simulated by STAR-2D, the scale length of plasma ablated by the pre-pulse is very short in overdense region and relatively longer in underdense region. Thus preformed plasmas with the scale length 10 μm are attached from $5n_{cr}$ point in addition to surface plasmas for the case with preformed plasmas. The p-polarized main pulse of the heating laser with 1.06 μm wavelength, $3x10^{19}$ W/cm^2 intensity and 16.5 μm spot diameter (Gaussian FWHM) irradiates the cone. The laser rises to its peak within 33 fs. Fast electron energy densities at 1 ps are shown in Figure 2 for both (a) without and (b) with preformed plasmas. For the case without preformed plasma, the central part of the main pulse directly hits the tip of the cone, and the surrounding parts are reflected at the sidewall of the cone and headed to the tip. Thus, most of fast electrons are generated at the tip. On the other hand, fast electrons are mainly generated in the underdense preformed plasma region and their energy is much higher than that without the preformed plasma case because of longer interaction length.

Energy coupling rates from the heating laser to all fast electrons or to low-energy (<10 MeV) fast electrons observed at the cone tip (15 μm width) are summarized in Table I. As the preformed plasma makes the distance from the generation point of fast electrons to the core longer than that without preformed plasmas, and fewer fast electrons can reach the core. Thus the energy coupling rate from the heating laser to fast electrons is reduced in the case with preformed plasmas. This reduction, however, is much significant, namely ~1/4 for the case to low-energy fast electrons, which are more suitable for heating the core. Therefore, coupling efficiency from the heating laser to the core is drastically degraded by the preformed plasma and it is indispensable to reduce the pre-pulse level as small as possible for efficient core heating. According to STAR-2D simulations, preformed plasmas are very localized around the cone tip when the pre-pulse intensity is $1x10^{11}$ W/cm^2 (*see Figure 1*), and we can expect very little effect of the preformed plasma. This means that we must reduce the pre-pulse level to ~1/100 compared with the current status.

TABLE I: ENERGY COUPLING RATES FROM LASER TO FAST ELECTRONS

	energy coupling rate [%]	
	to all	to low-energy (E<10 MeV)
without preformed plasma	48	39
with preformed plasma	36	11

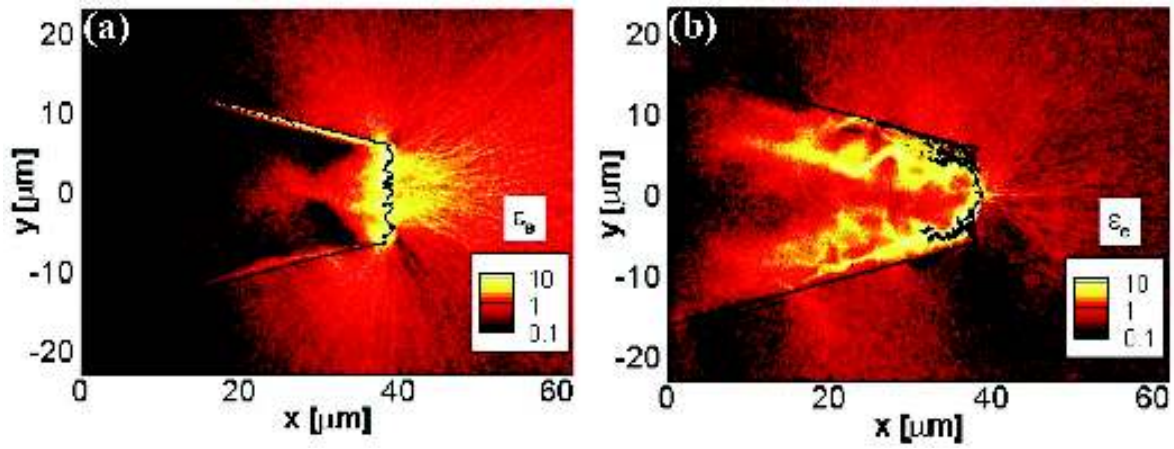

Figure 2: Fast electron energy densities at 1 ps for (a) without and (b) with preformed plasmas.

2.2 Thin Film Absorber

An amplified optical parametric fluorescence quencher [19] or a saturable absorber can be used to suppress the pre-pulse level. It is, however, still a technical challenge to maintain the pre-pulse intensity below $1x10^{11}$ W/cm^2. The other method to mitigate the pre-pulse problem, an entrance of the cone is suggested to be covered with an extremely thin film. The pre-pulse could be interrupted and absorbed by this film, and cannot irradiate the cone wall to produce long-scale preformed plasmas [17,18,20]. When the main pulse irradiates the cone, this film should be ionized by the pre-pulse and must diffuse to low density enough not to disturb the main pulse propagation. As the pulse duration of the pre-pulse is the order of nano second, plasmas have time to expand much below the critical density.

To evaluate remnant plasmas of the thin film, we performed STAR-2D simulations [18]. The thin film, which is made from CH and 0.1 μm thickness, is irradiated by the pre-pulse of $3x10^{11}$ W/cm^2 intensity, 100 μm spot diameter (Gaussian FWHM) and flattop temporal profile. Contour plots of the electron density are shown in Figure 3 at (a) 1.2 ns and (b) 1.8 ns. The electron density and the thickness of plasmas within the spot diameter along the laser axis become below 1/10 of the critical density and ~500 μm at 1.2 ns, 1/30 and 800 μm at 1.8 ns, respectively. Anyway, the main pulse must propagate through these very long rarefied plasmas.

3. Long Rarefied Plasma

3.1 Fast Electron Characteristics

To investigate effects of the long rarefied plasma inside the cone on fast electron characteristics, laser-plasma interactions are computed by FISCOF-1D using a time step of $5x10^{-3}$ fs, a resolution of 250 cells per laser wavelength, up to 200 particles per cell for electrons or ions. The heating laser is set to $I_L=10^{20}$ W/cm^2, λ_L=1.06 μm, τ_{FWHM}=1 ps Gaussian, and the Au (A=197, Z=30) cone tip is introduced as a 10 μm, $500n_{cr}$ flat profile, which is followed by 20 μm long CD ($500n_{cr}$, A=7, Z=3.5) plasma. We put the CH foam plasma ($10n_{cr}$, A=6.5, Z=3.5) with 50 μm thickness in front of the Au cone tip plasma to efficiently generate fast electrons [7]. We also put the H uniform plasma (A=1, Z=1, L_{rare}=150 or 300 μm thickness) with different densities ($n_{rare}=0.01n_{cr} \sim n_{cr}$) in front of the CH foam plasma as the long rarefied plasma. The

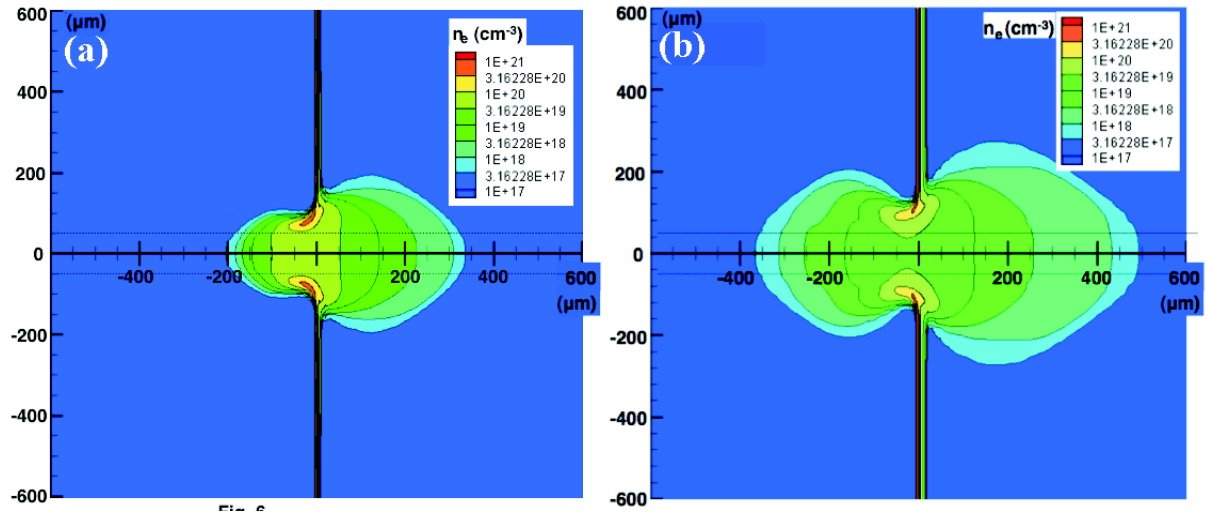

Figure 3: Electron density contour plots of remnant plasmas at (a) 1.2 ns and (b) 1.8 ns.

proton-electron mass ratio is set to1836, and initial temperatures of electrons and ions in all plasmas are set to 10 and 0.3 keV, respectively. A fast electron beam is observed in CD plasma,

10 μm behind the Au-CD boundary. To ignore a circulation of fast electrons that are reflected by the sheath field at the right edge of CD plasma, we introduce an artificial cooling region (7 μm long) at the rear of CD plasma, in which fast electrons are gradually cooled down to the initial temperature.

Time evolutions of fast electron beam intensity are shown in Figure 4 without rarefied plasmas and with rarefied plasmas of different densities (0.01, 0.05, 0.1, 0.5 and $1n_{cr}$) for (a) L_{rare}=150 and (b) 300 μm. As the intensity of the heating laser is 10^{20} W/cm^2, the fast electron beam intensity of 10^{19} W/cm^2 means that the instantaneous absorption rate from the laser to fast electrons is 10 %. Fast electron beam intensities are almost same as those in the case without rarefied plasmas for $n_{rare}<0.1n_{cr}$ with L_{rare}=150 μm and $n_{rare}=0.01n_{cr}$ with L_{rare}=300 μm. On the other hand, fast electron beam intensities become larger than that without rarefied plasmas due to large energy coupling rate from the laser to electrons for $n_{rare}>0.5n_{cr}$ with L_{rare}=150 μm and $n_{rare}>0.05n_{cr}$ with L_{rare}=300 μm. When the laser propagates within the plasma, a group velocity of light becomes slower as the density increases. So the leading edge of the fast electron beam delays more with the larger density of the rarefied plasma in the case of $n_{rare}>0.5n_{cr}$ with L_{rare}=150 μm, and the rarefied plasma with L_{rare}=300 μm enhances this delay much more. Total fast electron energies are calculated by time-integrating fast electron beam intensities and are shown in Figure 5 as a function of ρL n_{cr}·μm for both L_{rare}=150 and 300 μm, where ρ and L are the rarefied plasma density and thickness, respectively. In the case without rarefied plasmas (ρL =0), fast electrons are generated by interactions between the heating laser and the CH foam

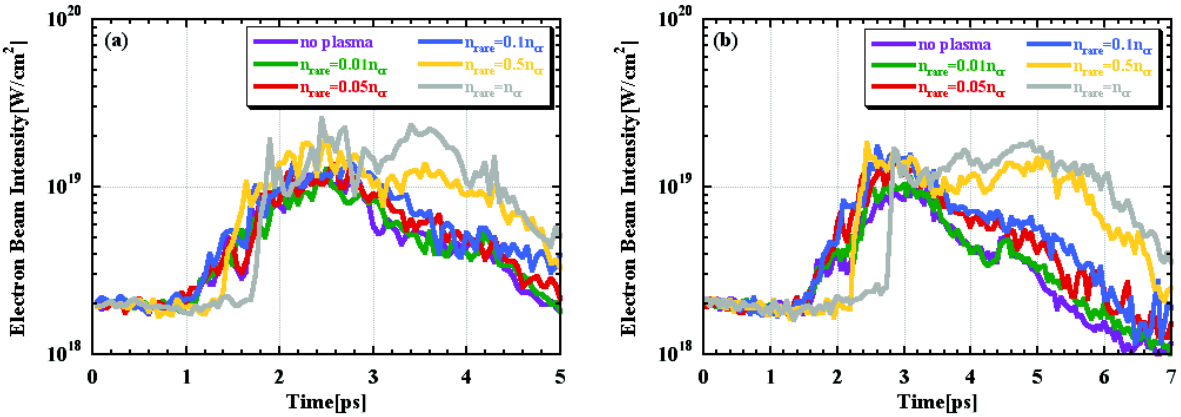

Figure 4: Time evolutions of fast electron beam intensity without rarefied plasmas and with rarefied plasmas of different densities (0.01, 0.05, 0.1, 0.5 and $1n_{cr}$) for (a) L_{rare}=150 and (b) 300 μm.

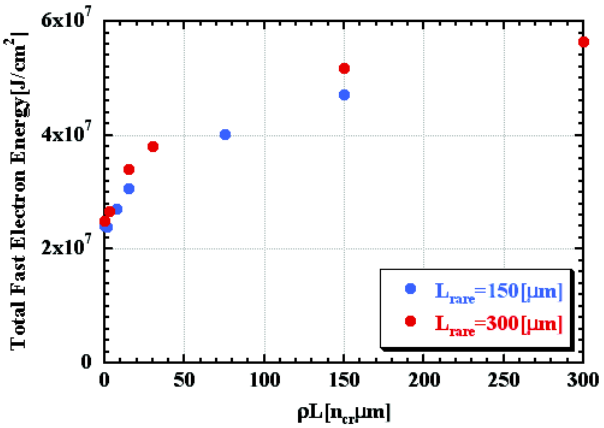

Figure 5: Total fast electron energies as a function of ρL n_{cr}·μm for both L_{rare}=150 and 300 μm.

plasma, and the total fast electron energy of ~2.4x10^7 J/cm^2 is obtained. If the rarefied plasma exists, the laser is absorbed within the underdense plasma and generates very energetic fast electrons. Thus energy increment of fast electrons is roughly proportional to ρL due to absorption increment up to ρL=150 n_{cr}·μm. When ρL is 300 n_{cr}·μm, the energy increment tends to saturate because the laser intensity decreases before irradiating the CH foam plasma due to large absorption and less fast electrons are generated.

Time averaged fast electron energy distributions are shown in Figure 6 without rarefied plasmas and with rarefied plasmas of different densities (0.01, 0.05, 0.1, 0.5 and 1n_{cr}) for (a) L_{rare}=150 and (b) 300 μm with wide energy range, and (c) L_{rare}=150 and (d) 300 μm with narrow energy range. When the density of the rarefied plasma is less than 0.1n_{cr} for L_{rare}=150 μm or 0.01n_{cr} for 300 μm, fast electron energy distributions are also same as those in the case without rarefied plasmas. If the density is greater than 0.5n_{cr} for L_{rare}=150 μm or 0.05n_{cr} for 300 μm, more laser energy is absorbed by the underdense rarefied plasma, and fast electrons with the energy more than 3 MeV are generated much more. They mainly contribute enhancement of the fast electron beam intensity (*see Figure 4*), however, these energetic fast electrons are not suitable for core heating at all. Fast electrons with the energy less than 2 MeV are strongly reduced in the case of n_{rare}=n_{cr} and L_{rare}=300 μm, because the heating laser is exhausted by the long rarefied plasma prior to reach the CH foam plasma and it can not generate many fast electrons.

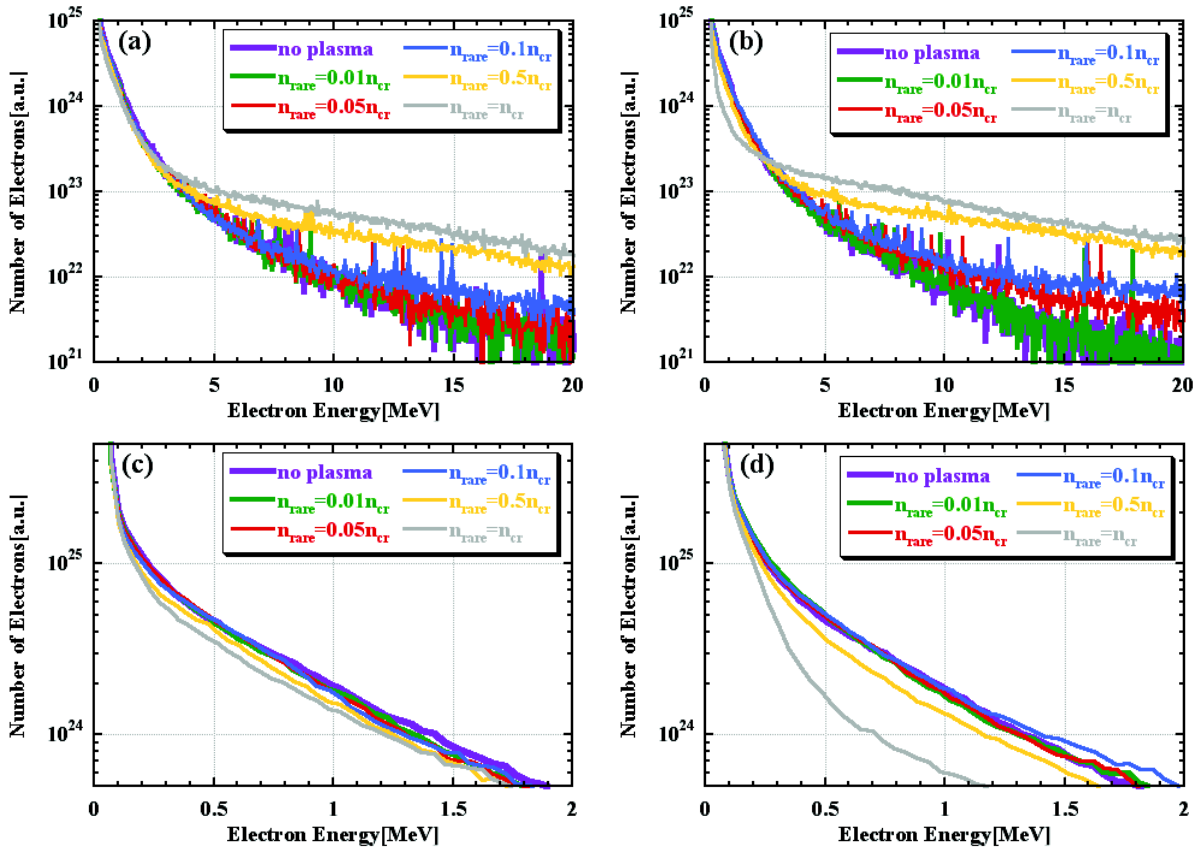

Figure 6: Time averaged fast electron energy distributions without rarefied plasmas and with rarefied plasmas of different densities (0.01, 0.05, 0.1, 0.5 and 1n_{cr}) for (a) L_{rare}=150 and (b) 300 μm with wide energy range, and (c) L_{rare}=150 and (d) 300 μm with narrow energy range.

3.2 Integrated Simulations for Core Heating

As the core heating is greatly affected by not only the beam intensity but also the energy distribution of fast electrons, we have performed FI^3 integrated simulations to estimate core temperatures, assuming the same core parameters as in Ref. 5. Observed fast electron profiles by FISCOF-1D in the previous section are used as the time-dependent momentum distributions of fast electrons for FIBMET-1D. Time evolutions of averaged core electron temperature computed by FIBMET-1D, which are averaged over the dense region (ρ>10 g/cm^3), are shown in Figure 7 without rarefied plasmas and with rarefied plasmas of different densities (0.01, 0.05, 0.1, 0.5 and 1n_{cr}) for (a) L_{rare}=150 and (b) 300 μm. Maximum averaged core electron temperatures are measured from Figure 7, and they are interpreted to reduction rate of a rise of the electron temperature. Degradations of electron temperature increment against the case without rarefied plasmas are shown in Figure 8 as a function of ρL n_{cr}·μm for both L_{rare}=150 and 300 μm. In the case of 150 μm thickness rarefied plasma, fast electrons that are suitable for core heating (< 2 MeV) are not affected so much by the rarefied plasma. (*see Figure 6 (c)*) Thus time evolutions are almost similar to the case without rarefied plasmas, and the maximum core electron temperature is only reduced by 15 % even for the n_{rare}=n_{cr} case. The electron temperature increment of the n_{rare}=n_{cr} and 300 μm thickness case is, however, strongly reduced and the degradation reaches more than 50 % because of much less appropriate fast electrons for core heating. (*see Figure 6 (d)*) If the degradation of less than 10 % is acceptable for the fast

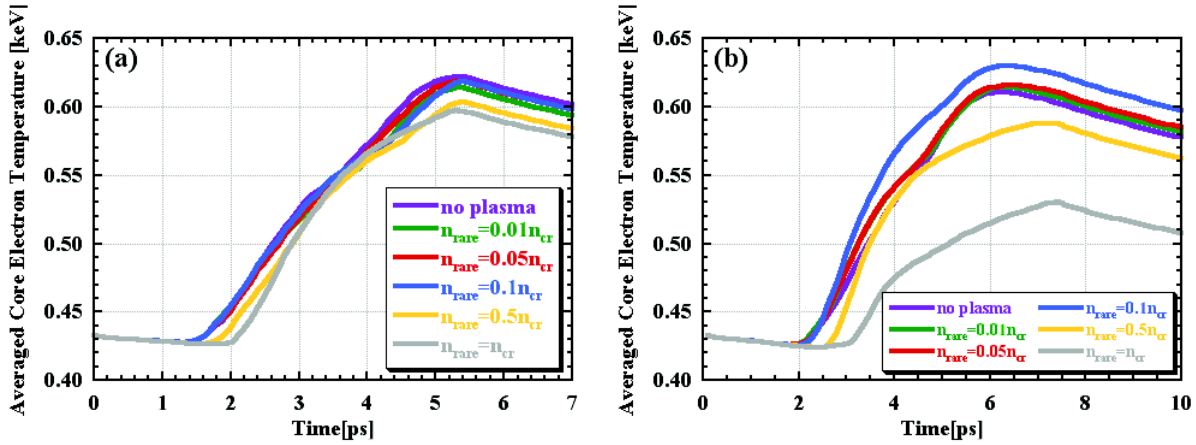

Figure 7: Time evolutions of averaged core electron temperature over the dense region (ρ>10 g/cm^3) without rarefied plasmas and with rarefied plasmas of different densities (0.01, 0.05, 0.1, 0.5 and 1n_{cr}) for (a) L_{rare}=150 and (b) 300 μm.

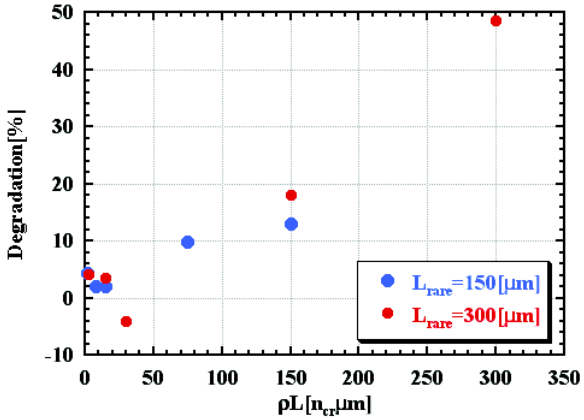

Figure 8: Degradations of electron temperature increment against the case without rarefied plasmas as a function of ρL n_{cr}·μm for both L_{rare}=150 and 300 μm.

ignition, ρL of the rarefied plasma must be smaller than 50 n_{cr}·μm. On the other hand, too small ρL plasma cannot absorb the pre-pulse and it hits the cone wall to generate long-scale

preformed plasmas. Therefore, we must optimize the film thickness against the pre-pulse intensity and more research is needed.

4. Summary

We estimated the pre-pulse energy, intensity and duration to be 130 mJ, 10^{13} W/cm^2 and 1 ns, respectively, by comparing simulation results with experimental observations. We simulated the pre-plasma formation inside the cone by the pre-pulse with above parameters and found that the inner space of the cone is filled with preformed plasmas. This is also suggested by the wide bright area away from the cone tip in X-ray pinhole images. After that, we performed simulations to evaluate preformed plasma effects inside the cone and found that the energy coupling rate from the laser to fast electrons especially suitable for core heating is drastically reduced due to the long-scale preformed plasma inside the cone.

To mitigate the serious problem of preformed plasmas, we proposed to introduce the thin film that covers an entrance of the cone. This method introduces long rarefied plasmas inside the cone, which could affect fast electron characteristics produced by the main pulse. Thus we investigated effects of long rarefied plasmas on fast electron generation and found that the electron beam intensity becomes larger than that without the rarefied plasma, but coupling efficiency from the heating laser to the core decreases due to lack of appropriate electrons for core heating. If the length the rarefied plasma is 500 μm (1 mm) and we can accept 10 % degradation of the core electron temperature, the thin film must be expanded by irradiation of the pre-pulse so that the density of the remnant rarefied plasma becomes less than $0.1n_{cr}$ ($0.05n_{cr}$).

Of course, the generation of fast electrons is simulated by 1D Particle-in-Cell code in this paper, multi-dimensional analyses including laser beam filamentation, phase distortion, diverging and merging in underdense plasma are needed to clarify our conclusion.

Acknowledgements

This work is partially supported by JSPS Grant-in-Aid for Scientific Research (C)(22540511).

References

[1] AZECHI, H. and FIREX PROJECT, “The FIREX Program on the Way to Inertial Fusion Energy”, J. Phys.: Conf. Series **112** (2008) 012002.
[2] SAKAGAMI, H., MIMA, K., “Interconnection between Hydro and PIC codes for Fast Ignition Simulations”, Laser Part. Beams **22** (2004) 41-44.
[3] NAKAMURA, T., SAKAGAMI, H., JOHZAKI, T., NAGATOMO, H., MIMA, K., “Generation and transport of fast electrons inside cone targets irradiated by intense laser pulses”, Laser Part. Beams **24** (2006) 5-8.
[4] SAKAGAMI, H., JOHZAKI, T., NAGATOMO, H., MIMA, K., “Fast ignition integrated interconnecting code project for cone-guided targets”, Laser and Particle Beams **24** (2006) 191-198.
[5] JOHZAKI, T., SAKAGAMI, H., NAGATOMO, H., MIMA, K., “Holistic Simulation for FIREX Project with FI^3”, Laser Part. Beams **25** (2007) 621-629.
[6] NAKAMURA, T., MIMA, K., SAKAGAMI, H., JOHZAKI, T., NAGATOMO, H., “Generation and confinement of high energy by irradiation of ultra-intense short laser pulses onto cone targets”, Laser Part. Beams **26** (2008) 207-212.

[7] SAKAGAMI, H., JOHZAKI, T., NAGATOMO, H., MIMA, K., "Generation control of fast electron beam by low density foam for FIREX-I", Nucl. Fusion **49** (2009) 075026.
[8] KODAMA, R. et al., "Fast heating scalable to laser fusion ignition", Nature **418** (2002) 933.
[9] MIMA, K., et al., "FIREX project and effects of self-generated electric and magnetic fields on electron-driven fast ignition", Plasma Phys. Control Fusion **52** (2010) 124047.
[10] JOHZAKI, T., et al., accepted in Nucl. Fusion.
[11] KEMP, A.J., SENTOKU, Y., TABAK, M., "Hot-electron energy coupling in ultraintense laser-matter interaction", Phys. Rev. E **79** (2009) 066406.
[12] NAGATOMO, H., OHNISHI, N., MIMA, K., SAWADA, K., NISHIHARA, K., TAKABE, H., "Analysis of Hydrodynamic Instabilities in Implosion using High-accuracy Integrated Implosion Code", Proc. 2nd Int. Conf. on Inertial Fusion Sciences and Applications (Kyoto, Japan, 9-14 Sept. 2001), Elsevier, Paris (2002) 140-142.
[13] SUNAHARA, A., SASAKI, A., NISHIHARA, K., "Two Dimensional Radiation Hydrodynamic Simulation for Extreme Ultra-Violet Emission from Laser-produced Tin Plasmas", J. Phys.: Conf. Series **112** (2008) 042048.
[14] SAKAGAMI, H., MIMA, K., "Fast Ignition Simulations with Collective PIC Code", Proc. 2nd Int. Conf. on Inertial Fusion Sciences and Applications (Kyoto, Japan, 9-14 Sept. 2001), Elsevier, Paris (2002) 380-383.
[15] CAI, H.B., MIMA, K., ZHOU, W.M., JOHZAKI, T., NAGATOMO, H., SUNAHARA, A., MASON, R.J., "Enhancing the Number of High-Energy Electrons Deposited to a Compressed Pellet via Double Cones in Fast Ignition", Phys. Rev. Lett. **102** (2009) 245001.
[16] JOHZAKI, T., NAGATOMO, H., SAKAGAMI, H., SENTOKU, Y., NAKAMURA, T., MIMA, K., NAKAO, Y., YOKOTA, T., "Core heating analysis of fast ignition targets by integrated simulations", J. Phys. IV **133** (2006) 385-389.
[17] MIMA, K., et al., "FIREX project and effects of self-generated electric and magnetic fields on electron-driven fast ignition", Plasma Phys. Control. Fusion **52** (2010) 124047.
[18] SUNAHARA, A., et al., submitted to Laser Part. Beams.
[19] KONDO, K., et al., "Control of amplified optical parametric fluorescence for hybrid chirped-pulse amplification", J. Opt. Soc. Am. B **23** (2006) 231-235.
[20] KINOSHITA, K., et al., "Propagation of an intense femtosecond laser pulse through a thin foil filter", App. Phys. Lett. **84** (2004) 4623-4625.